

We are IntechOpen, the world's leading publisher of Open Access books Built by scientists, for scientists

6,900

Open access books available

186,000

International authors and editors

200M

Downloads

Our authors are among the

154

Countries delivered to

TOP 1%

most cited scientists

12.2%

Contributors from top 500 universities



WEB OF SCIENCE™

Selection of our books indexed in the Book Citation Index
in Web of Science™ Core Collection (BKCI)

Interested in publishing with us?
Contact book.department@intechopen.com

Numbers displayed above are based on latest data collected.
For more information visit www.intechopen.com



Field Estimation through Ray-Tracing for Microwave Links

Ada Vittoria Bosisio

National Research Council of Italy, CNR/IEIIT c/o Politecnico di Milano
Italy

1. Introduction

Engineers using microwave radio links have to address the effects of multipath propagation that arise when several rays arrive at the receiver after travelling along different paths from the transmitter. Rays, along their propagation, undergo reflections at the earth's surface or at variations in the refractive index or its gradient.

Since the '60s, standard ray theories for radio wave applications use effective earth radius concepts, ray bending based on Snell's law in a layered spherical atmosphere, or analytical method, limited to simple refractive index profiles (Du Castel, 1966; Livingston, 1970). At that time, scientists were interested in statistics of fading, distinguishing between *fast* or *slow fading* and the typical results were either nomograms of attenuation as a function of distance for a set of common frequency and height values or cumulative distribution functions representing the fraction of time that the signal was expected to be received at or below a given level (CCIR, 1978). Several techniques were employed to calculate the field strength, such as Cornu's spiral derived by the Huygens' principle together with the introduction of the specular and the diffuse reflection contribution (Hall, 1979). In that approach, the field amplitude was determined assuming the principle of conservation of energy, i.e. the flux of the energy along a ray is the same at every cross section of a narrow tube of rays (Keller, 1957).

Nowadays, radio communications live a renaissance due to the development of mobile and wireless communications and the increasing demand of wideband services. The need of greater rate of transmission is accomplished using higher frequencies for which effects like the tropospheric scatter can affect dramatically the quality of the received signal. Thus, aspects such as analysis of delay power spectra or of potential intersystem interferences require a more realistic modelling. As a matter of fact, local fluctuations in the refractive index n can cause scatter, while its abrupt changes with the height can cause reflection and originate ducting layers, in which the rays are reflected and refracted back in such a way that the field is trapped inside these layers (Bean & Dutton, 1968).

Although the goal of radio engineering is to transmit reliably from the source to the receiver, this is of no use if the received signal is unintelligible due to interference or if the transmission causes interference with other systems. So an analysis of the channel behaviour is mandatory to meet both link design and system requirements. Besides, the availability of geographic databases, digital elevation models and the increasing computing power let us face more realistic description to model the interaction of the propagating wave with the atmosphere and the surrounding scenario (Driessen, 2000; Kurner & Cichon, 1993; Lebherz et al., 1992).

In more recent developments, ray modelling of wave propagation addresses the dispersive effects of perturbed atmosphere on the performance of high-capacity digital radio channel (Akbarpour & Webster, 2005; Sevgi & Felsen, 1998).

Besides telecommunications applications, a proper modelling of atmospheric propagation is of concern in atmospheric sciences with particular focus on radio occultation data analysis for assimilation with numerical weather prediction models (Pany et al., 2001). Also, the decrease of propagation speed related to the atmospheric refractivity causes tropospheric delay, which influences applications of the Global Navigation Satellite System (Eresmaa et al., 2008).

The author presents a widely diffuse technique in the domain of seismic studies that accommodates lateral variations in the medium properties (Farra, 1993). As an asymptotic technique, based on high frequency approximation, it permits fast computation but provides a local solution of propagation problem (Červený et al., 1977). The technique was adapted for application with electromagnetic waves and specifically tailored for signals travelling in the atmosphere. The hypothesis of horizontal uniformity can be removed and no stratification is needed to calculate the ray trajectory. The terrain profile coordinates are mapped over a Cartesian reference through analytical transformation. Refractive index values are given in the same Cartesian reference. Hence, propagation is modelled in a two dimensional range-height scenario over irregular terrain through non-homogeneous atmosphere.

The field amplitude is evaluated by means of a perturbation technique using paraxial rays to observe the wave front structure along the path from the transmitter towards the receiver.

This approach allows to analyze system performance and the channel impulse response in presence of any kind of atmosphere, characterized by local values of refractive index n in the bi-dimensional panel including the antennae and the terrain profile. The variations of the refractive index n along the third dimension are taken equal to zero; nonetheless, the field amplitude is calculated correctly because of the paraxial approximation which takes place in a 3D domain. Median power strength of the numerical results was compared with predictions given by Friis' Formula (Balanis, 1996).

2. Modelling

The proposed ray tracing technique is widely used in seismic for subsoil investigation and it follows an approach based upon the integration of the Eikonal equation with Hamiltonian-Jacobi technique (Kružkov, 1975). According to this formulation, rays are defined by the vector $y(\tau) = (x(\tau), p(\tau))$, where $x(\tau)$ and $p(\tau)$ are the position vector and the slowness (inverse of phase velocity) vector along the ray, both function of the integration variable τ and of the initial conditions (launching point and direction). The slowness vector p is defined as \mathbf{k} / ω and $e^{jk \cdot x}$ is the phase function. The vector $y(\tau)$ satisfies the Hamilton differential equations, whose solutions describe the wave propagation in the medium, under the asymptotic assumption (Abramovitz & Stegun, 1970):

$$\begin{cases} \frac{dx}{d\tau} = \nabla_p \mathcal{H} \\ \frac{dp}{d\tau} = -\nabla_x \mathcal{H} \end{cases} \quad (1)$$

where ∇_p and ∇_x represent the gradient computed versus the slowness vector and the position vector, respectively. \mathcal{H} is the Hamiltonian function describing the wave propagation in the considered medium, i.e. the atmosphere, chosen as follows:

$$\mathcal{H}(x, p) = \frac{1}{2}(v^2(x)p^2 - 1) \quad (2)$$

being $v(x)$ the propagation speed of the medium at the position vector x .

The advantage of such an approach is twofold: it takes into account the medium inhomogeneities that originate multipath propagation and wavefronts folding (caustics), and it permits to consider both vertical and long range variations of the atmospheric model, without any approximation like flat-earth model (Hall, 1979). Also, it permits to keep separated the different field contributions due to the different interactions between the rays and the surrounding scenario, which impacts on the phase calculation of the overall received field.

2.1 Ray tracing

A suitable discussion for ray tracing can be found in (Farra, 1993); nevertheless, in this section some basic concepts and analytical details are reported.

Substituting (2) in (1), one obtains the equations for the vector $y(\tau)$:

$$\begin{cases} \frac{dx}{d\tau} = pv^2(x) \\ \frac{dp}{d\tau} = -\frac{\nabla_x v(x)}{v(x)} \end{cases} \quad (3)$$

x and p define the 6D phase-space, where the solution of (3), i.e. the rays, are the characteristic lines of the Eikonal equation, thus enabling the interpolation without ambiguity on a single fold (Vinje et al., 1993). For this reason rays are also called bi-characteristics lines of the wave equation. By choosing as integration variable the ray propagation delay or travel time T , system (3) becomes:

$$\begin{cases} \frac{dx}{dT} = c^2(x)p_x \\ \frac{dy}{dT} = c^2(x)p_y \\ \frac{dz}{dT} = c^2(x)p_z \\ \frac{dp_x}{dT} = \frac{1}{c^2(x)} \frac{\partial c(x)}{\partial x} \\ \frac{dp_y}{dT} = \frac{1}{c^2(x)} \frac{\partial c(x)}{\partial y} \\ \frac{dp_z}{dT} = \frac{1}{c^2(x)} \frac{\partial c(x)}{\partial z} \end{cases} \quad (4)$$

The solution of system (4) describes, under the asymptotic assumption, the propagation in the atmosphere in terms of ray trajectories and time delay.

2.2 Amplitude calculation

Anomalous conditions such as medium inhomogeneity or velocity model variations can affect dramatically the wavefront propagation. Under these circumstances the computation based upon the spherical divergence assumption results in erroneous evaluations.

One possible choice is to compute the amplitude through paraxial rays (first order perturbation theory), used to determine the flow tube, whose deformations, together with the theorem of the conservation of the flux along the ray path, allow the calculation of the amplitude A at the time τ .

Let us consider a reference ray with characteristic vector $\mathbf{y}_0(\tau) = (\mathbf{x}_0(\tau), \mathbf{p}_0(\tau))$. A paraxial ray is obtained from the reference one by applying the first order perturbation theory, so paraxial rays coordinates are defined by:

$$\begin{aligned} \mathbf{x}(\tau) &= \mathbf{x}_0(\tau) + \delta\mathbf{x}(\tau) \\ \mathbf{p}(\tau) &= \mathbf{p}_0(\tau) + \delta\mathbf{p}(\tau) \end{aligned} \quad (5)$$

Tracing paraxial rays consists in finding in the phase-space the canonical perturbation vector $\delta\mathbf{y}(\tau) = (\delta\mathbf{x}(\tau), \delta\mathbf{p}(\tau))$. These perturbations in the trajectory are due to small changes in the initial conditions of the ray.

The linear system for the calculation of paraxial rays is obtained by inserting the perturbation vector given by (5) in system (1) and developing to the first order:

$$\frac{d\delta\mathbf{y}}{d\tau} = \mathbf{A}(\tau) \cdot \delta\mathbf{y} \quad (6)$$

where

$$\mathbf{A} = \begin{bmatrix} \nabla_{\mathbf{x}} \nabla_{\mathbf{p}} H & \nabla_{\mathbf{p}} \nabla_{\mathbf{p}} H \\ -\nabla_{\mathbf{x}} \nabla_{\mathbf{x}} H & -\nabla_{\mathbf{p}} \nabla_{\mathbf{x}} H \end{bmatrix} \quad (7)$$

is a 6×6 matrix whose elements are the derivatives of the Hamiltonian function calculated on the reference ray.

Paraxial rays allow to define the *flow tube*, schematically represented in figure 1.

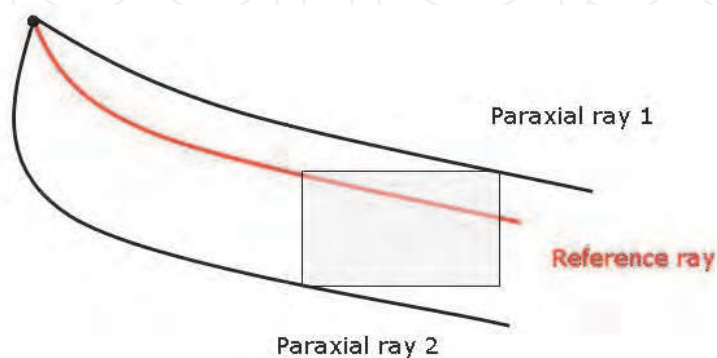


Fig. 1. Flow tube definition through paraxial ray tracing

The deformation of the flow tube along the ray path ℓ is given by the jacobian J :

$$J = \frac{\partial(x, y, z)}{\partial(\tau, \vartheta, \phi)} = \det \begin{bmatrix} \frac{\partial x}{\partial \tau} & \frac{\partial x}{\partial \vartheta} & \frac{\partial x}{\partial \phi} \\ \frac{\partial y}{\partial \tau} & \frac{\partial y}{\partial \vartheta} & \frac{\partial y}{\partial \phi} \\ \frac{\partial z}{\partial \tau} & \frac{\partial z}{\partial \vartheta} & \frac{\partial z}{\partial \phi} \end{bmatrix} \quad (8)$$

where τ is the sampling parameter, θ the elevation angle and ϕ the azimuth angle. The amplitude of the plane wave associated to the ray is computed considering both the deformation of the flow tube and the conservation of power density flow law along the ray path. The volume element of the flow tube can be expressed as $dV = J d\tau d\vartheta d\phi$ or $dV = dS d\ell$. Thus, the elementary surface dS has the following expression:

$$dS = \frac{dV}{d\ell} = \frac{J d\tau d\vartheta d\phi}{d\ell} = \frac{J}{v} d\vartheta d\phi \quad (9)$$

From the conservation of the power density flow along the ray (Keller, 1957) and known the amplitude A_i at τ_i , it follows that the amplitude A_{i+1} at τ_{i+1} is:

$$A_{i+1} = A_i \frac{v_{i+1}}{v_i} \sqrt{\frac{J_i}{J_{i+1}}} \quad (10)$$

Equation (10) shows that the ray amplitude depends on the velocity model. Hence, paraxial rays take into account anomalous propagation conditions.

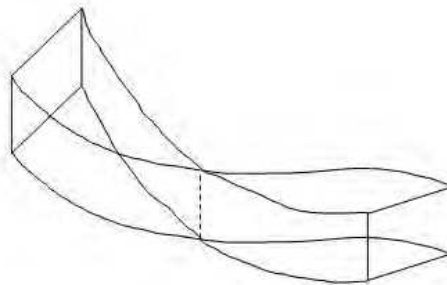


Fig. 2. Sketch of a caustics of the first order: the flow tube loses one dimension

The singularity of the Jacobian J is a singularity, known as *caustic*, of the plane wave associated to the ray (Kravtsov & Orlov, 1990). Caustics arise when the ray field folds. Caustics are of first order when the flow tube loses one dimension and of the second order when two are the dimensions lost. The wave front folding affects the phase of the field carried by the wave with a phase shift of $\pi/2$ radians for each caustic order. These events are carefully accounted so that the proper phase shifts can be applied to the field.

2.3 Parameterization

The modelling is performed in a 2D panel, as far as the terrain profile and the atmosphere characteristics are concerned, while the ray trajectories are computed in a 3D space.

This assumption is based on the hypothesis that lateral variations in the propagation medium and in the terrain profile are negligible in the third dimension, which does not strictly holds.

Therefore, the propagation occurs in the so called *Earth system* (s,h) , where s is the range measured along the idealized spherical earth and h is the altitude taken along radial direction passing through the Earth centre, respectively. Instead, for sake of simplicity, all calculation are developed in a Cartesian reference system (x,z) related to the Earth by the following transformation relationships:

$$\begin{aligned} x &= (R_0 + h) \sin\left(\frac{s}{R_0}\right) \\ z &= (R_0 + h) \cos\left(\frac{s}{R_0}\right) - R_0 \end{aligned} \quad (11)$$

where R_0 is the Earth radius. The transformation from cartographic coordinates (s,h) to absolute coordinates (x,z) is given by the inverse transformation:

$$\begin{aligned} s &= R_0 \arctan\left(\frac{x}{z + R_0}\right) \\ h &= \sqrt{x^2 + (z + R_0)^2} - R_0 \end{aligned} \quad (12)$$

being $\theta = s / R_0$ the angle at the centre of the Earth, as shown in figure 3.

This way to proceed allows to take into account the actual geometry of the problem without introducing approximations like equivalent Earth radius. Also, it keeps separated the domain in which the radio link characteristics are defined and the computational one, where rays are traced.

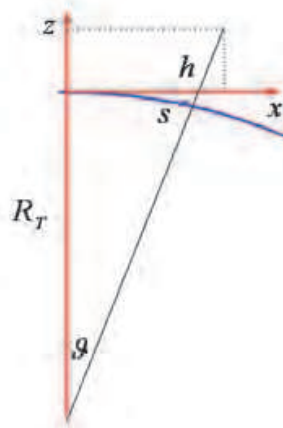


Fig. 3. The two reference systems: cartographic coordinates (s,h) and absolute ones (x,z) .

The characteristics of the atmosphere are taken into account in terms of its propagation velocity using several quantities that are generally function of the position vector \mathbf{x} :

$$v(x) = \frac{c}{n(x)} = \frac{1}{p(x)} \quad (13)$$

where c is the speed of the light and $n(x)$ is the refractive index of the atmosphere, which usually is expressed in terms of the refractivity N :

$$N = (n - 1) \cdot 10^6 \quad (14)$$

N is a dimensionless quantity but in literature it is often measured in N -units or in parts per million (ppm). Its value depends upon the altitude and the range locally according to the atmospheric pressure P , the vapour pressure P_V and the temperature T as in the following (Bean and Dutton, 1968) :

$$N = 77.6 \frac{P}{T} + 3.73 \cdot 10^5 \frac{P_V}{T^2} \quad (15)$$

Besides the variations in the refractive index, or its gradient, rays along their propagation undergo reflections and diffraction at the earth's surface. At the present stage of the modelling, neither the diffraction mechanisms nor any scattering features are included except reflection.

The trajectory of the reflected ray is given by the Snell's law under the hypothesis that locally the ground acts as a perfect smooth surface. The initial conditions with which the reflected ray is traced depend both on the geometric characteristics of the terrain profile and on the ray direction of incidence. The amplitude and the phase of the rays reflected from the ground are computed according to the chosen ground parameterization, i.e. the electric soil properties. These determine the value of the ground impedance η , which is a function of both soil permittivity ϵ_r and conductivity σ (Ulaby, 1999):

$$\eta = \sqrt{\frac{\mu}{\epsilon_0 \epsilon_r}} \left(1 - j \frac{\sigma}{\omega \epsilon_0 \epsilon_r} \right) \quad (16)$$

being ϵ_0 and ω the free space permittivity and the angular frequency respectively.

Once that the rays trajectories are computed, together with their complex amplitudes - weighted by the antenna pattern - and the travel times, they are classified into different wave fronts and then interpolated on the locations where the field is desired. The total field is obtained by addition of the single contribution of each wave front.

3. Received field estimation

The field reconstruction is described by means of a pilot example of a 4.5 GHz point-to-point radio link 80 km long affected by multipath. The aim of the technique is to evaluate the vertical electric field (or the received power) intensity at the receiver range. According to the considered geometry, this leads to the prediction of the vertical profile of the electric field $E(h)$ (or $P(h)$), where h is the receiver height ranging between $(h_0 - \Delta h / 2)$ and $(h_0 + \Delta h / 2)$.

In the following we refer to this interval of width Δh as *target zone* or simply *target*.

The modelled atmospheric condition is indicated in the panel of figure 4, while figure 5 shows the vertical profile of N at few chosen distances. The N value is comprised between

280 and 360 N-units and it shows variations in both dimensions. This atmospheric model - taken from (Bean and Dutton, 1968), p.325 - let us focus on several kind of interactions and their effects on the propagating signal that could possible occur in actual conditions.

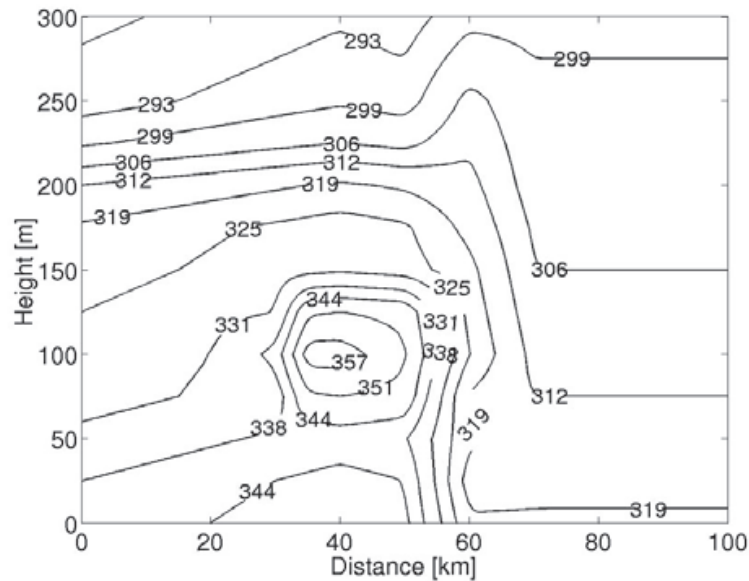


Fig. 4. 2D panel of the atmosphere characteristics. Contour lines report the value of the refractivity index N

To appreciate the role of the variations in the refractivity, and without loss of generality, the ground profile was chosen as a plane surface characterized by the values of permittivity $\epsilon_r = 3$ and conductivity $\sigma = 0.001$ [S/m] in the frequency band of interest.

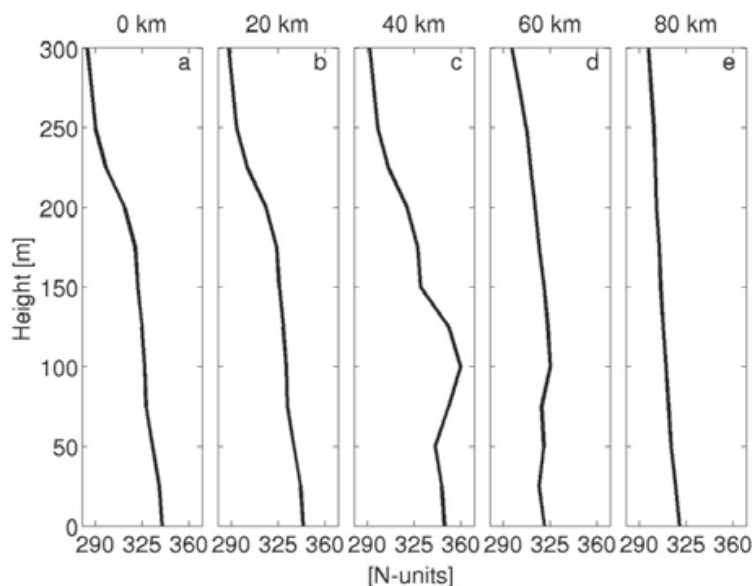


Fig. 5. Vertical profile at 5 chosen range distances.

The top image in figure 6 shows the trajectories of the rays belonging to a chosen elevation angular sector ($-0.5^\circ \div 0.5^\circ$ with respect to the local horizon) traced in the cartographic

system. The transmitter is in the origin of abscissas axis at 100 m above the ground. Besides the wavefront that carries the direct arrival of the signal, one may observe that several wavefronts are involved, resulting from the inhomogeneities of the atmosphere and ground reflection.

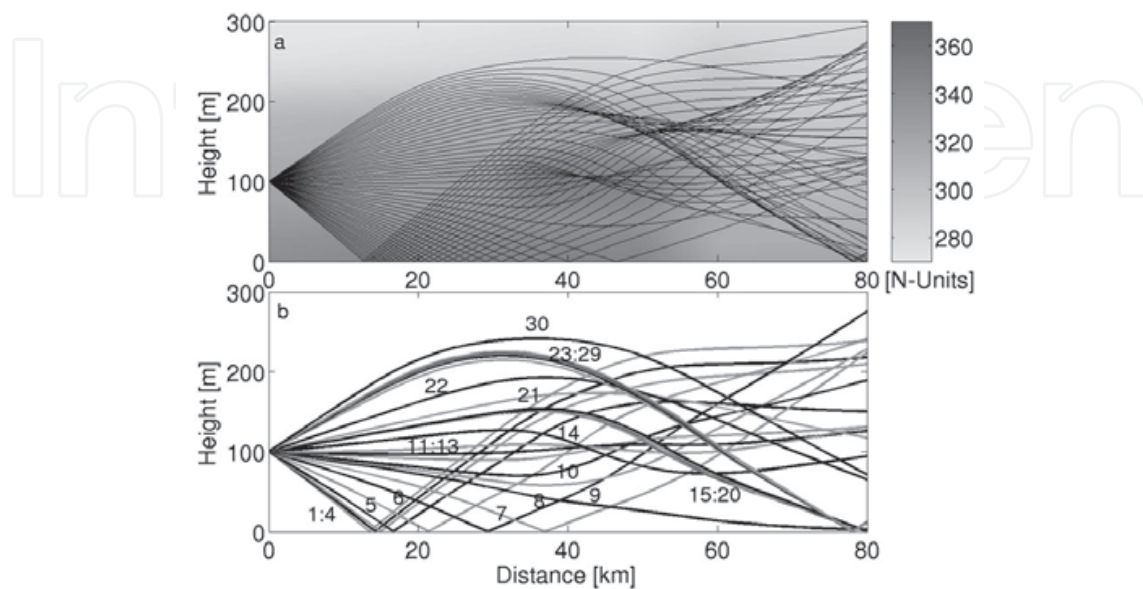


Fig. 6. Ray pattern (top) and wavefronts (bottom)

The bottom image of figure 6 shows the rays pertaining to the 30 wavefronts that results from the ray tracing process. The first step consists in grouping rays in different wave fronts, each characterized by the same *history* such as same number and location of caustics or reflections. Wavefronts are numbered and rays belonging to the same wavefront can be used to interpolate the field. As a matter of fact, rays arrive at the receiver range at discrete values so that the vertical profiling of the field intensity involves three steps: wavefronts separation; interpolation of the ray comb belonging to the same wavefront; coherent addition of the wavefronts themselves.

3.1 Wave front separation

The first criterion of wavefront separation that could come in mind is that of the travel time arrivals. Figure 7a shows the multi-valued behaviour of the wavefront delay of arrivals at different heights, while figure 7b shows how the parameterization of the wavefronts in the ray launching angle resolves the ambiguity: working in the angle domain seems the natural way for unfolding multi-valued ray fields (Operto et al., 2000).

The wavefronts separation is based on a broad and on a narrow selection process applied consecutively. The broad selection process involves the ray history: as for example, two rays belong to two different wavefronts if they are reflected a different number of times. The narrow selection process uses as criterion the *angular distance*: if two rays are reflected the same number of times they belong to the different wavefronts when their elevation starting angles difference is greater than $\delta\theta$. This angular distance has the role of guarantee the proper accuracy in the interpolation of the ray field and it depends on the velocity model of the medium (Sun, 1992).

The results of the wavefront separation process are organized in a database whose structure is schematically represented in figure 8. Wavefronts and rays are organized in a record frame that gives for the k^{th} wavefront the propagation delay τ_k , the amplitude A_k and the phase ϕ_k obtained by interpolation of the travel time T_{ik} , a_{ik} and ϕ_{ik} of the rays at their arrival height, where i pertains to the individual rays in the wavefront k .

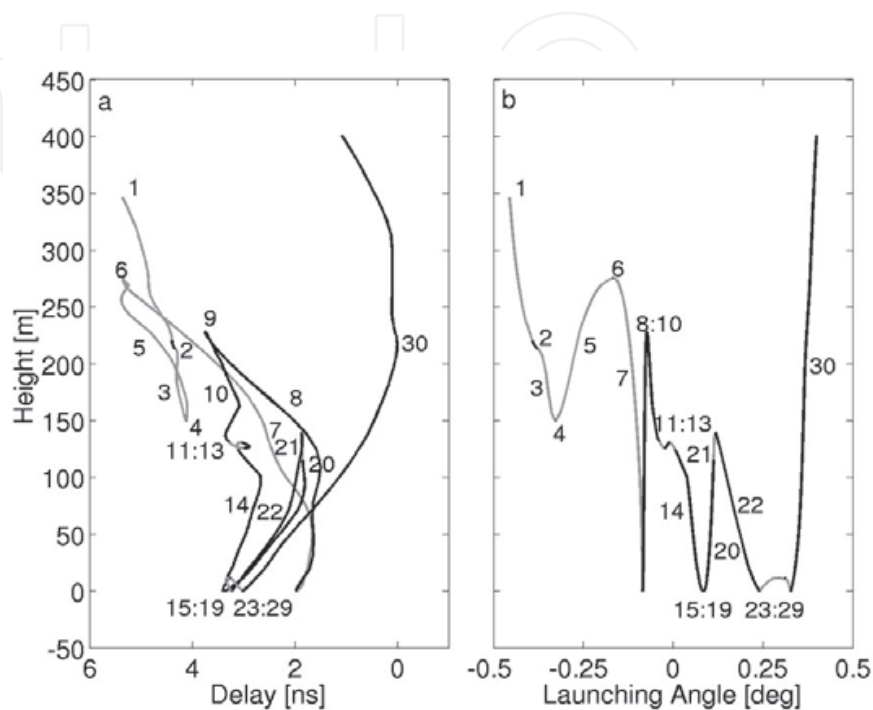


Fig. 7. Wavefronts time delay dispersion (a) and launching angle distribution (b)

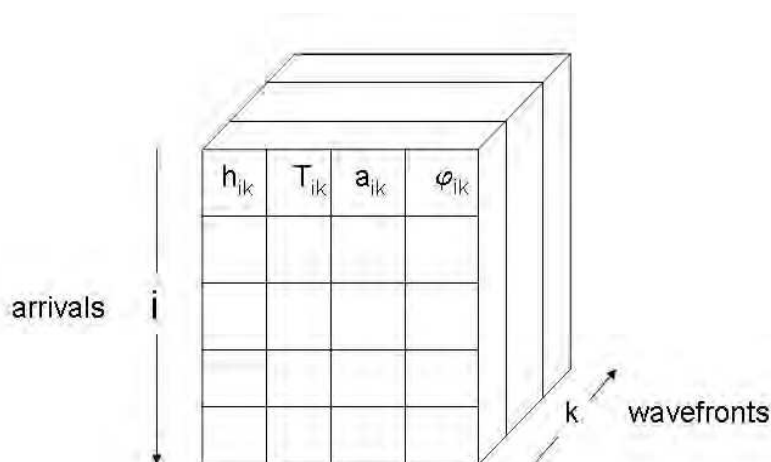


Fig. 8. Ray field database: the arrivals are organized according to their wavefronts

Each ray record refers is composed of the following parameters: the height of arrival, the travel time, which depend on the ray *history*; the amplitude and the phase, which depend on the ray *history*, on the reflection coefficients and on the system parameters.

The various quantities calculated by the ray tracing are referred to as Green's function attributes. Figure 9 shows among the attributes those that directly contribute to the field calculation.

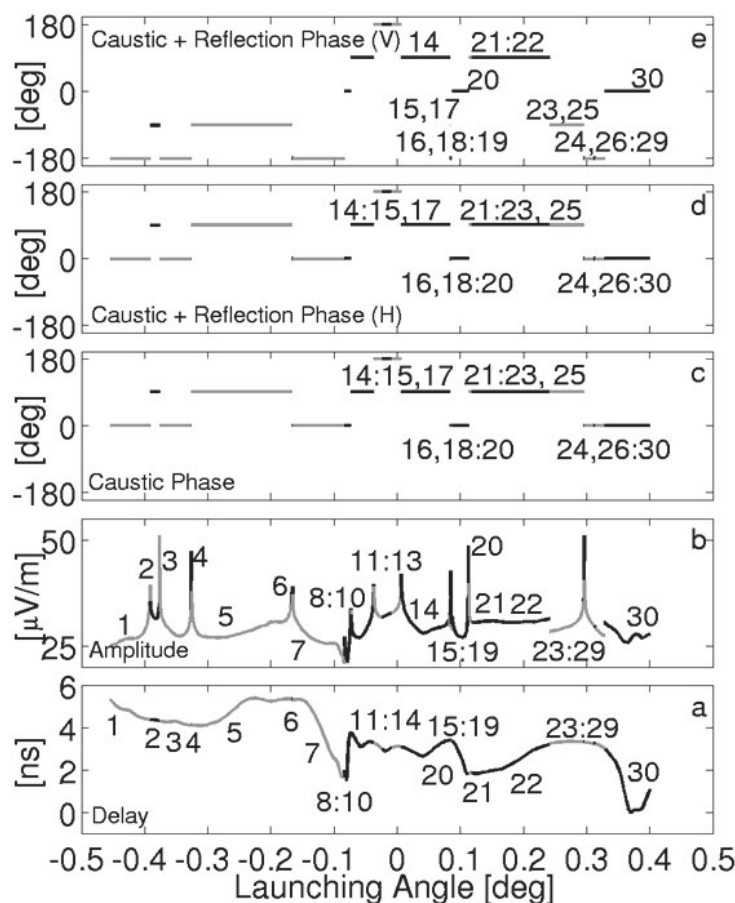


Fig. 9. Green's function attributes for the field calculation: from bottom to top: delay(a), amplitude (b), caustic phase (c), caustic +reflection phase (H polarization), caustic + reflection phase (V polarization)

3.2 Wave front interpolation

The field calculation along the vertical profile at the receiver range is performed through the interpolation of the different wavefronts contribution. Let K be the number of the wavefronts, each including N_k arrivals, the electric field associated to the i^{th} arrival of the k^{th} wavefront is:

$$\mathbf{E}(h_{ik}) = a_{ik} e^{j(2\pi f_0 T_{ik} + \phi_{ik})} \equiv \mathbf{E}_{ik} \quad (17)$$

where f is the frequency of operation of the link. The contribution of the k^{th} wavefront to the total field is obtained through interpolation of the travel times, of the amplitudes and of the phases in the following way:

$$\mathbf{E}_k(h) = g_k(\mathbf{E}_{1k}, \mathbf{E}_{2k}, \dots, \mathbf{E}_{N_k k}) \quad (18)$$

where g_k is a generic interpolating function and h is the height. As result, the interpolation of local values returns the field intensity in the target zone. Finally, the overall field is computed adding coherently all the wavefronts contributions:

$$\mathbf{E}(h) = \sum_{k=1}^K \mathbf{E}_k(h) \quad (19)$$

The vertical profile of the received power is obtained by applying locally the Poynting's theorem to a spherical surface with radius R :

$$P(h) = \frac{4\pi R^2}{\eta} |\mathbf{E}(h)|^2 \quad (20)$$

being η the medium impedance and R the receiver range.

The solid line in the leftmost panel of figure 10 shows the power profile due to the direct arrival, while the dotted line represents the theoretical values predicted by Friis' formula (Balanis, 1996). Here, the vertical power profile is shown along the entire computational domain, from 0 up to 300 m, in order to show the effects of the tropospheric multipath on the received signal. The panel in the middle and the rightmost one of figure 10 show the power profile computed adding all the wavefront contribution at vertical (V) and horizontal (H) polarization.

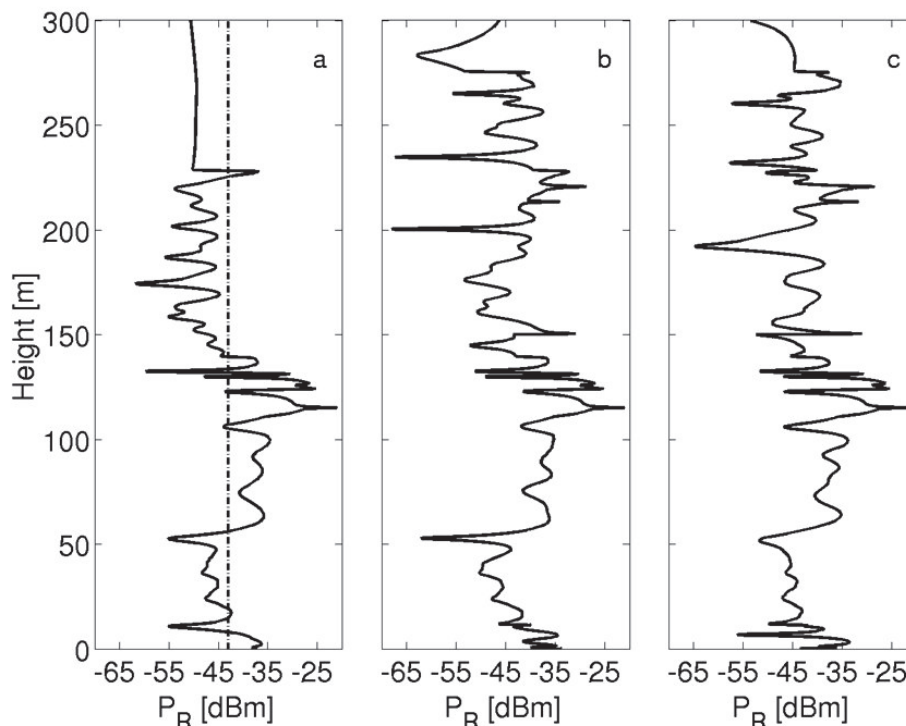


Fig. 10. Received Power vertical profile, from left to right: direct arrival contribution (solid line) and theoretical arrive (Friis); direct + reflected contribution (vertical polarization); direct + reflected contribution (horizontal polarization)

4. Radio channel analysis

4.1 Time domain approach

The aim of time domain approach is to estimate the radio channel response to a transmitted pulse with a given waveform $s(t)$. The use of the analytical extension concept let treat correctly the two distinct phase contributions of each arrival, i.e. the first one due to the propagation delay and the second one due to caustics and reflections, if any. The analytical extension of a base band signal $s(t)$ is given by:

$$\tilde{s}_{BB}(t) = s(t) + jH\{s(t)\} \quad (21)$$

where H represents the Hilbert transform operator. The corresponding pass band signal, which is transmitted on radio channel, is obtained with a frequency shift:

$$\tilde{s}_{RF} = \tilde{s}_{BB}(t)e^{j2\pi f_0 t} \quad (22)$$

The channel pulse response can be written as a sequence of ideal shifted pulses of the transmitted waveform with their own amplitude and phase:

$$w(t) = \sum_{k=1}^K A_k e^{j\phi_k} \delta(t - \tau_k) \quad (23)$$

where the amplitudes, the phases and the propagation delays have been calculated, respectively, through interpolation of a_{ik} , ϕ_{ik} and T_{ik} at height h . These procedure has low computational cost as the ray trajectories and propagation delay τ_k do not depend on the frequency and they can be computed once for all. In equation (23) some quantities such as amplitudes A_k and phases ϕ_k depends on the frequency of operation but using a narrow band approximation one can assume that amplitude and phase variations are negligible within the signal bandwidth. Under these hypothesis, the pass band received signal $\tilde{u}_{RF}(t)$ is given by the convolution between the pass band transmitted signal $\tilde{s}_{RF}(t)$ and the channel response (23):

$$\tilde{u}_{RF}(t) = \sum_{k=1}^K A_k e^{j\phi_k} \delta(t - \tau_k) \tilde{s}_{BB}(t - \tau_k) e^{j2\pi f_0 (t - \tau_k)} \quad (24)$$

The received base band signal $\tilde{u}_{BB}(t)$ is obtained multiplying the pass band signal $\tilde{u}_{RF}(t)$ by the exponential $e^{-j2\pi f_0 t}$:

$$\tilde{u}_{BB}(t) = \sum_{k=1}^K A_k e^{j\phi_k} \tilde{s}_{BB}(t - \tau_k) e^{-j2\pi f_0 \tau_k} \quad (25)$$

whose real part gives the received signal $u(t)$:

$$u(t) = \text{Re}\{\tilde{u}_{BB}(t)\} \quad (26)$$

The panel in figure 11 reports the estimated field and the time delay as a function of height ranging between $(h_0 - \Delta h / 2)$ and $(h_0 + \Delta h / 2)$, being $h_0 = 125$ m and $\Delta h = 25$ m observed at

the receiver range. This represents the impulse response of the system computed at vertical polarization. The input signal is a Nyquist wavelet and it is drawn in the left image of figure 11 as a dotted line. Also, figure 11 shows the received signal (solid line) at four given height of the panel. Two in-phase but slightly delayed arrivals are evident in panel a). In panel b) there are 2 arrivals, with one of them with a $\pi/4$ phase shift, while in panel d) the arrivals are of opposite phase.

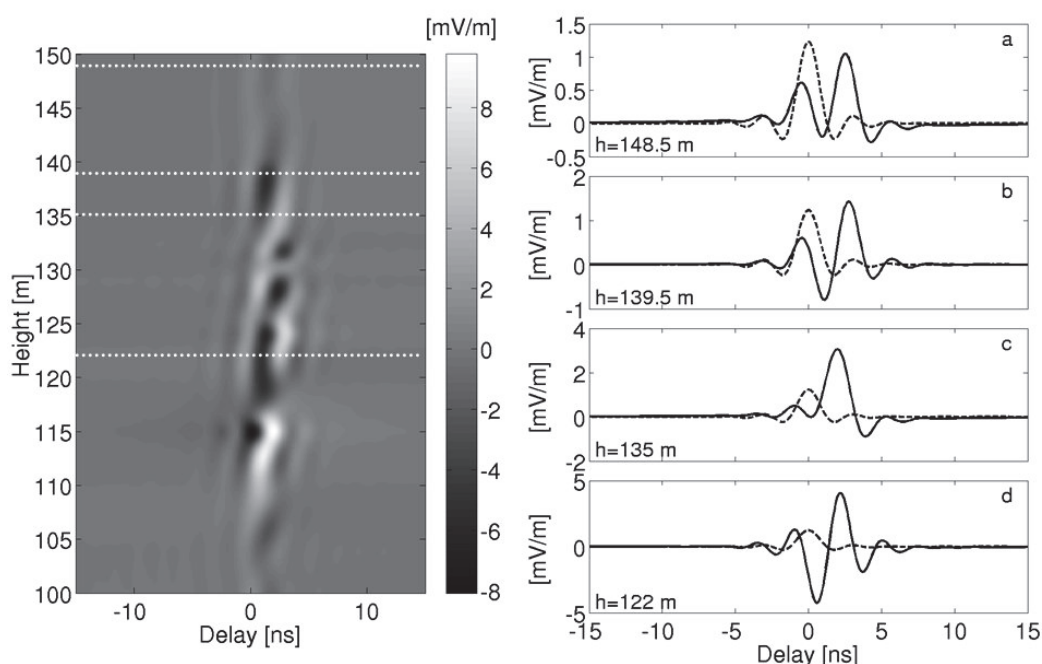


Fig. 11. Impulse response panel (left). The image on the right shows the channel response to the transmitted Nyquist wavelet at four height values, sketched as a dotted white line in the panel on the left.

4.2 Frequency domain approach

The computation of the electric field in the target zone for a given frequency f_0 as reported in §3.2 strictly holds under the hypothesis of the transmission of a sinusoidal signal, which has an infinite duration and an infinitesimal band. As radio systems transmit signals with finite duration and band, there is the need to evaluate the response of the radio channel to the effects of frequency variation inside the system bandwidth of operation.

Let us assume that the radio link is transmitting a signal with bandwidth B around the carrier frequency f_0 . Therefore, given the frequency f and using the equation (17) principle, the received electric field expression is:

$$E(f) = \sum_{k=1}^K A_k e^{j(2\pi f \tau_k + \phi_k)} \quad (27)$$

Applying equation (27) for each frequency in the interval spanning from $(f_0 - B/2)$ to $(f_0 + B/2)$ one obtains an estimate of the pass band radio channel transfer function. The evaluation of equation (27) at different frequencies requires to update the amplitude terms

A_k and the phase terms ϕ_k , which both depends (directly or indirectly) on the frequency of operation f .

Frequency domain approach can lead also to a characterization of radio channel in the time domain applying Fourier transform to the radio channel transfer function provided by equation (27). However, when the bandwidth of the transmitted signal is narrow, that is when $f_0 \gg B$, this procedure leads to a waste of computational resources. A more efficient way to manage narrow band channels is to face the problem in the time domain.

The transfer function of the radio channel is shown in figure 12 together with the frequency behaviour computed at the same four height levels highlighted in the time domain analysis. Again the target zone is comprised between 100 and 150 m and the signal has vertical polarization. One can notices how the transfer function may change from a smooth behaviour, panel c) to a sharper one with a notch deepness of about 30 dB, panel a).

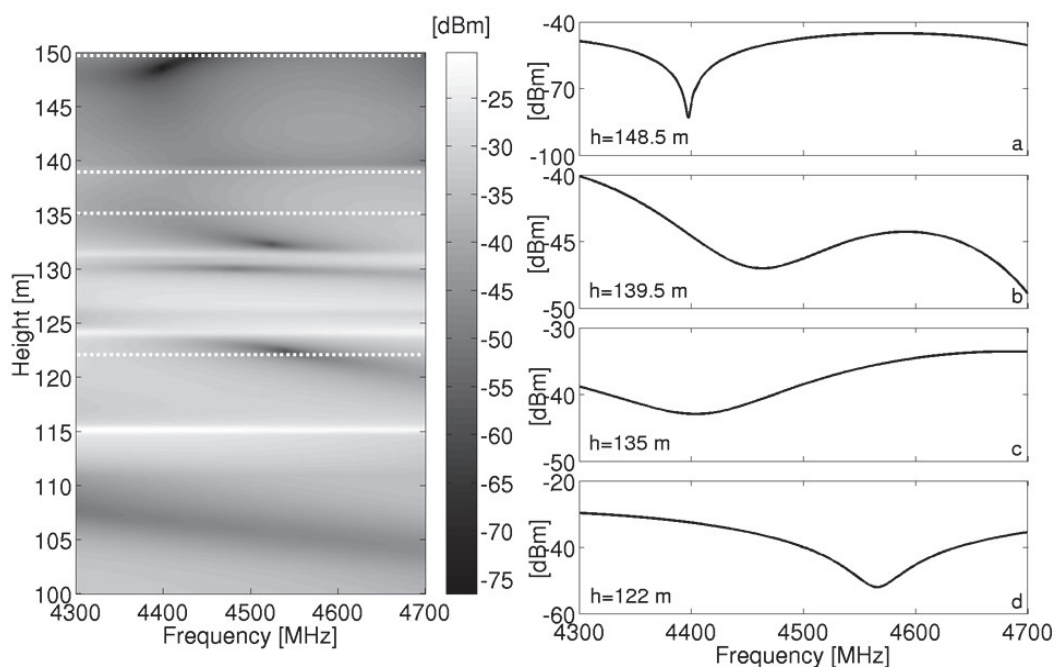


Fig. 12. Transfer function panel (left). The image on the right shows the channel response to the transmitted Nyquist wavelet at four height values, sketched as a dotted white line in the panel on the left.

5. Numerical validation

The ray tracing technique was developed to set up a prediction tool that is operative both as a MATLAB-based package and a C++ executable code. Unfortunately, beside an industrial application whose results are not available for publication at this stage, the computed field and power vertical profiles were not validated against measurements. Nevertheless the quality of the prediction performance can be observed when compared against canonical scenarios or other authors reference solutions.

Usually, when developing solver codes, one starts with the comparison of the predicted results with analytical or assessed solutions to check the correctness of the implementation. If this is the proper choice at that stage, it could lead to a flat and formal exposition of the methodology under study when describing the single steps towards the overall result. That

is why the particular example chosen to illustrate the technique throughout §3 and §4 is far complicated, as it appears from the number and variety of wavefronts and from the aspects of the radio link characteristics both in time and in frequency domain. As the complexity could conceal errors or misvaluations, the author chose as reference solution an example in which a standard atmosphere model describes the velocity of the propagation medium over a flat perfect electric conductor ground. Even in such a simple example, the importance of the wave front discrimination could induce in errors when reconstructing the field.

5.1 Two ray example

The transmitter, in the origin of the abscissa axis, is at 150 m above the ground and the receiver range is 50 km apart. The atmospheric model is a standard exponential one with a gradient of 40 ppm in the first 1000m. Figure 13 shows the trajectories together with the two wavefront, one associated with the direct arrival and another with the reflected one. The ground is a perfect conductor with reflection coefficient equal to -1.

The two arrivals, direct and reflected, are shown in figure 14: on the leftmost panel the wavefront time delay dispersion results in 2 distinct contribution at the same instant. As in §3.1, the parameterization in the angular domain nicely unfolds the integration path (rightmost panel).

The predicted vertical received power profile is reported in figure 15, together with the direct arrival contributions given by Friis' formula. One can notice the typical pattern of zero and maxima of reception due to the rotating in-phase and counter-phase summation of the two arrivals.

Finally, figure 16 shows the impulse response panel calculated for the two ray model and vertical polarization. Again, the received signal shows different behaviour due to the atmospheric multipath as a function of the height.

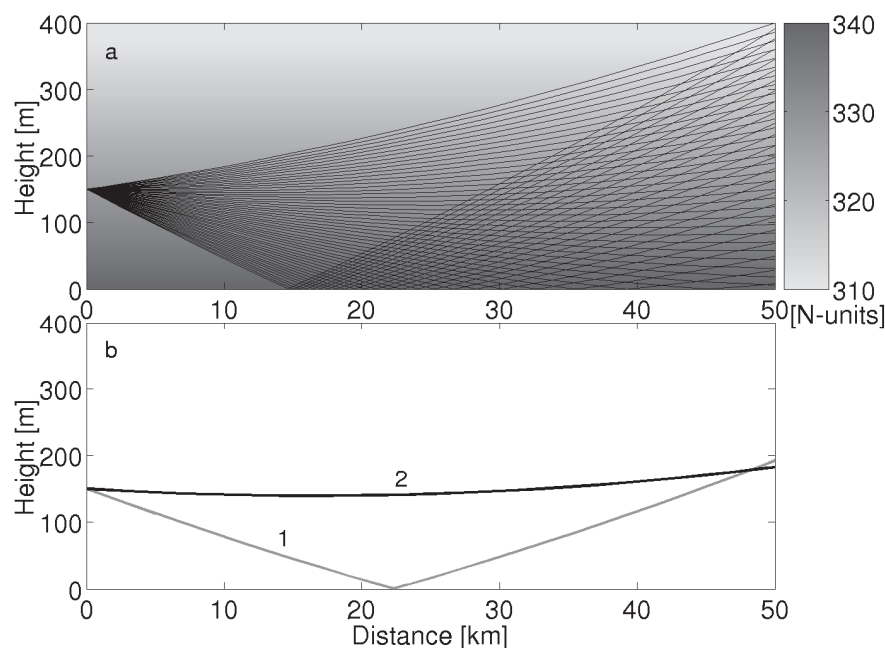


Fig. 13. Ray pattern (top) and wavefronts (bottom)

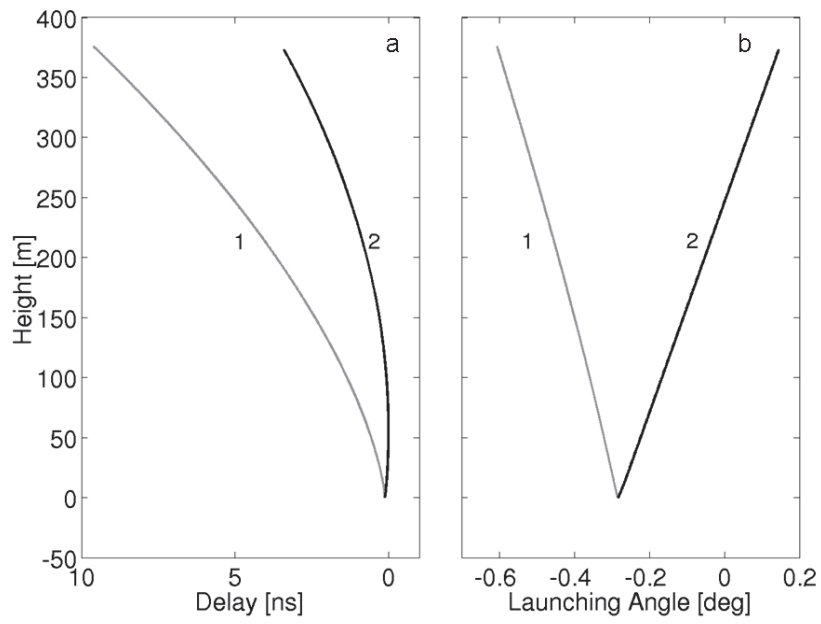


Fig. 14. Wavefronts time delay dispersion (a) and launching angle distribution (b)

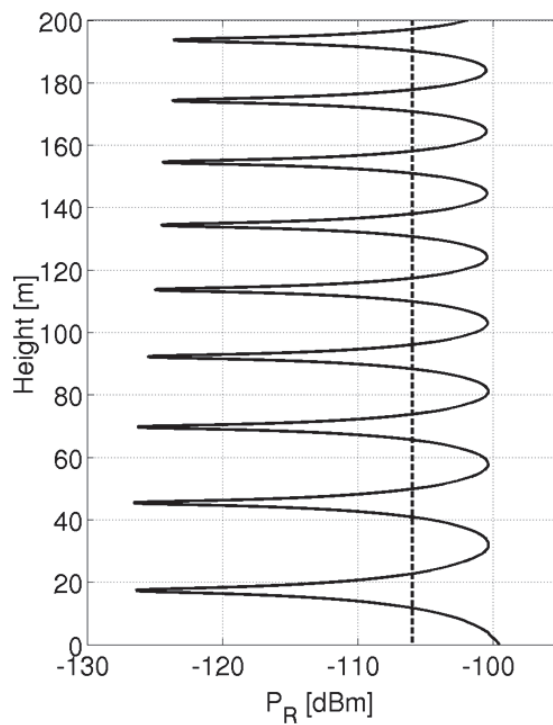


Fig. 15. Received Power vertical profile (solid line) and direct arrival (dotted line)

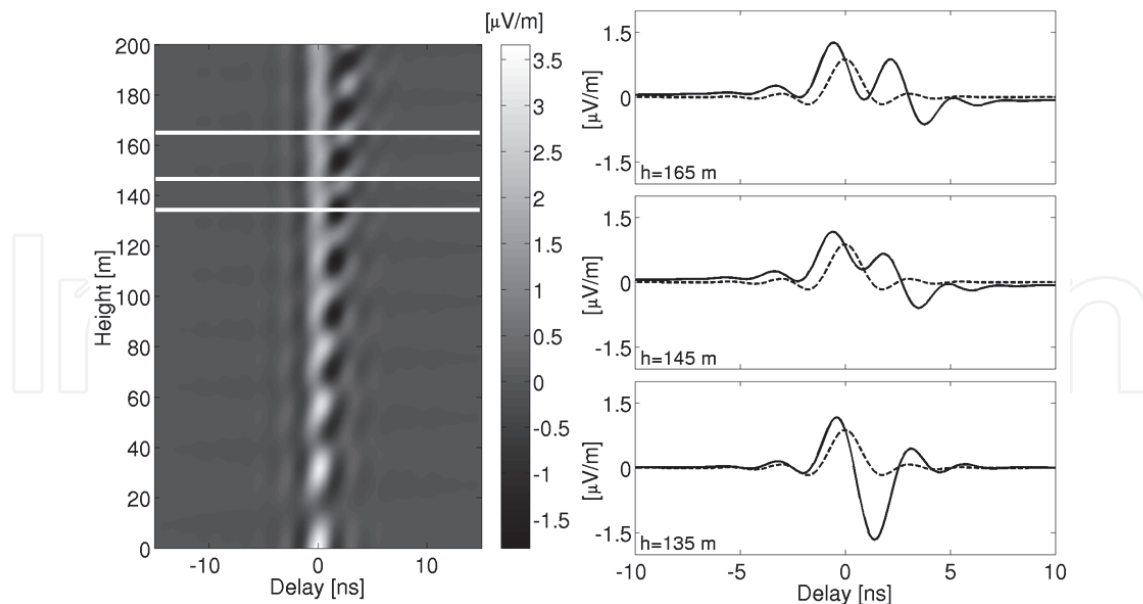


Fig. 16. Impulse response panel (left). The image on the right shows the channel response to the transmitted Nyquist wavelet at three height values, sketched as a white line in the panel on the left.

6. Conclusion

The ray tracing technique based on the resolution of the Eikonal equation with Hamilton-Jacobi technique is well suited to model the dispersive effects of perturbed atmosphere on the performance of high-capacity digital radio channel.

The advantage of such an approach is the possibility of describing the medium with its variation in the lateral domain in presence of atmospheric multipath and of non uniform terrain profile.

The field profiling at the receiving site is obtained through 2,5D propagation as, notwithstanding all variations in the third dimension are taken equal to zero, the field amplitude is calculated correctly because of the paraxial approximation which takes place in a 3D domain.

At the time of writing the author is refining the code towards a full 3D implementation, which requires a reformulation in spherical coordinates, and the modelling of the mechanism of ground scattering and diffraction.

7. Acknowledgment

The author would like to thank Professor Giuseppe Drufuca (Politecnico di Milano) for his useful comments and suggestions and Simone Re (former research associate, Politecnico di Milano) for his contribution to the code development and calculations.

8. References

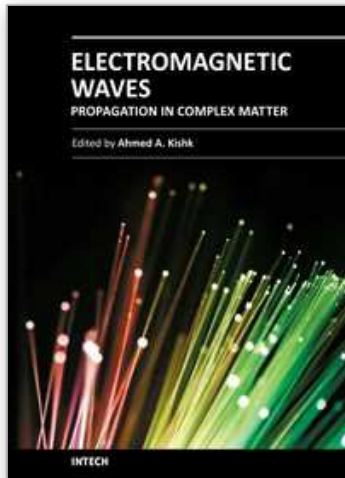
Abramovitz M., Stegun I.A. (1970), *Handbook of mathematical functions*, Dover Publications, New York (USA).

- Akbarpour R., Webster A.R., Ray-Tracing and parabolic Equation Methods in the Modeling of a Tropospheric Microwave Link, *IEEE Transactions on Antennas and Propagation*, Vol.53, No.11, (November 2005), pp. 2785-3791, ISSN 0018-926X.
- Balanis C. A (1996), *Antenna Theory: Analysis and Design*, John Wiley & Sons, ISBN 0471592684, New York (USA).
- Bean B. R., Dutton E.~J.(1968), *Radio Meteorology*, Dover Publications, New York (USA)
- CCIR, Report 338, Propagation Data and Prediction Methods Required for Line-of-Sight Radio Relay Systems, *Study Group 5 of the International Consultative Radio Committee (CCIR)*, Geneva (CH), 1978.
- Červený V. I.A. Molotkov, I. Psencik (1977), *Ray method in Seismology*, Univerzita Karlova Praha.
- Driessen P.F., Prediction of multipath delay profiles in mountainous terrain, *IEEE Journal on Selected Areas in Communications*, Vol.18, No.3, (March 2000), pp.336-346, ISSN 0733-8716.
- Du Castel (1966), *Tropospheric Radiowave propagation beyond the Horizon*, Pergamon Press, Oxford (UK).
- Eresmaa R., Healy S., Järvinen H., Salonen K., Implementation of a ray-tracing operator for ground-based GPS Slant Delay observation modelling, *Journal of Geophysical Research*, Vol.113, D11114, doi:10.1029/2007JD009256, (June 2008), 9 pages , ISSN 0148-0227.
- Farra V., Ray Tracing in Complex Media, *Journal of Applied Geophysics*, Vol.30, No.1-2, (April 1993), pp. 55-73, ISSN 0926-9851.
- Hall M. P. M.(1979), *Effects of the troposphere on radio communication*, IEEE Electromagnetic Waves Series, ISBN 0-906048-25-7, Exeter, UK.
- Keller J.B., Diffraction by an Aperture, *Journal of Applied Physics*, Vol. 28, No. 4, (April 1957), pp 426-444.
- Kravtsov Y.A., Orlov Y.I (1990), *Geometrical Optics of Inhomogeneous Media*, Springer-Verlag, ISBN 3-540-51944-0, New York (USA).
- Kružkov S. N., Generalized solutions of the Hamilton-Jacobi equations of Eikonal type I. Formulation of the problems; existence, uniqueness and stability theorems; some properties of the solutions, *Mathematics of the USSR-Sbornik*, Vol. 27, No. 3, (1975), pp. 406-446.
- Kurner T., Cichon D. J., Concepts and results for 3D digital terrain-based wave propagation models: an overview, *IEEE Journal on Selected Areas in Communication*, Vol.11, No.7, (September 1993), pp.1002-1012, ISSN 0733-8716.
- Lebherz M., Wiesbeck W., Krank W., A Versatile wave propagation model for the VHF/UHF range considering three-dimensional terrain, *IEEE Transactions on Antennas and Propagation*, Vol.40, No.10 (October 1992), pp 1121-1131, ISSN 0018-926X.
- Livingston D.C. (1970). *The physics of microwave propagation*, Prentice Hall, New Jersey (USA).
- Operto M.S., Xu S., Lambaré G., Can we quantitatively image complex structures with rays?, *Geophysics*, Vol. 65, No. 4, (July August 2000), pp. 1223-1238, ISSN 0016-8033.
- Pany T., Pesec P., G. Stangl, Atmospheric GPS Slant Path Delays and Ray Tracing through Numerical Wather Models, a Comparison, *Physics and Chemistry of the Earth, Part A: Solid Earth and Geodesy*, Vol.26, No.3, (2001), pp.183-188, ISSN 1474-7065.
- Sevgi L., Felsen L.B., A New Algorithm For Ground Wave Propagation Based On A Hybrid Ray-Mode Approach, *International Journal of Numerical Modelling*, Vol.11, No.2, (March-April 1998), pp. 87-103, Online ISSN 1099-1204.

- Sun Y., Computation of 2D multiple arrival travel time fields by an interpolative shooting method, SEG Annual Meeting, Extended Abstracts (1992), pp 156-159, Tulsa (OK), USA.
- Ulaby F.T. (1999), Fundamentals of applied electromagnetics, Prentice Hall, ISBN 0-13-011554-1, New Jersey (USA).
- Vinje V., Iversen E., Gjoystdal H., Travelttime and amplitude estimation using wavefront construction, *Geophysics*, Vol. 58, No. 6, (August 1993), pp. 1157-1166, ISSN 0016-8033.

IntechOpen

IntechOpen



Electromagnetic Waves Propagation in Complex Matter

Edited by Prof. Ahmed Kishk

ISBN 978-953-307-445-0

Hard cover, 292 pages

Publisher InTech

Published online 24, June, 2011

Published in print edition June, 2011

This volume is based on the contributions of several authors in electromagnetic waves propagations. Several issues are considered. The contents of most of the chapters are highlighting non classic presentation of wave propagation and interaction with matters. This volume bridges the gap between physics and engineering in these issues. Each chapter keeps the author notation that the reader should be aware of as he reads from chapter to the other.

How to reference

In order to correctly reference this scholarly work, feel free to copy and paste the following:

Ada Vittoria Bosisio (2011). Field Estimation through Ray- Tracing for Microwave Links, Electromagnetic Waves Propagation in Complex Matter, Prof. Ahmed Kishk (Ed.), ISBN: 978-953-307-445-0, InTech, Available from: <http://www.intechopen.com/books/electromagnetic-waves-propagation-in-complex-matter/field-estimation-through-ray-tracing-for-microwave-links>

INTECH
open science | open minds

InTech Europe

University Campus STeP Ri
Slavka Krautzeka 83/A
51000 Rijeka, Croatia
Phone: +385 (51) 770 447
Fax: +385 (51) 686 166
www.intechopen.com

InTech China

Unit 405, Office Block, Hotel Equatorial Shanghai
No.65, Yan An Road (West), Shanghai, 200040, China
中国上海市延安西路65号上海国际贵都大饭店办公楼405单元
Phone: +86-21-62489820
Fax: +86-21-62489821

© 2011 The Author(s). Licensee IntechOpen. This chapter is distributed under the terms of the [Creative Commons Attribution-NonCommercial-ShareAlike-3.0 License](#), which permits use, distribution and reproduction for non-commercial purposes, provided the original is properly cited and derivative works building on this content are distributed under the same license.

IntechOpen

IntechOpen